Appendix A. Supplementary Content

Optimization of graphene-based materials outperforming host epoxy matrices

L. GUADAGNO[A]*, M. RAIMONDO[A], L. VERTUCCIO[A], M. MAURO[B], G. GUERRA[B], K. LAFDI[C], B. DE VIVO[D], P. LAMBERTI[D], G. SPINELLI[D], V. TUCCI[D]

[a] *Department of Industrial Engineering, University of Salerno, Via Giovanni Paolo II 132, Fisciano (SA) 84084, Italy*

[b] *Department of Chemistry and Biology, University of Salerno, Via Giovanni Paolo II 132, Fisciano (SA), 84084, Italy*

[c] *University of Dayton, 300 College Park, Dayton Ohio, 45440, USA*

[d] *Department of Information Engineering, Electrical Engineering and Mathematics Applied University of Salerno, Via Giovanni Paolo II 132, Fisciano (SA), 84084, Italy*

Carbon nanofiller characterization

Graphene layers embedded inside polymeric materials promise more fascinating physics applications, but one of the major obstacle to understand and drive the behavior of the nanofilled polymer is the absence of a reliable or a single method to produce graphene sheets or exfoliated graphite. In literature, graphene and exfoliated graphite used to impart functional properties or simply as reinforcement for the polymer, were produced using different procedure and then different structure, functionalizations and morphological features. For this reason, it is really necessary an accurate characterization of the nanofiller with different techniques to understand the correlations between structural and morphological organization of graphene-based materials and physical and mechanical properties of the nanofilled resins. In this paper an accurate and detailed characterization of the nanofiller was performed before to analyze the properties of the nanofilled resins.

X-Ray Diffraction Analysis

X-ray diffraction patterns of fully exfoliated graphite (SL) and partially exfoliated graphite (pEG), carboxylated partially exfoliated graphite (CpEG) are shown in Figure 1S. The diffraction pattern of SL sample is typical of completely exfoliated graphite, in fact no reflections of crystalline phases are observed. CpEG and pEG diffractgrams were added for comparison.
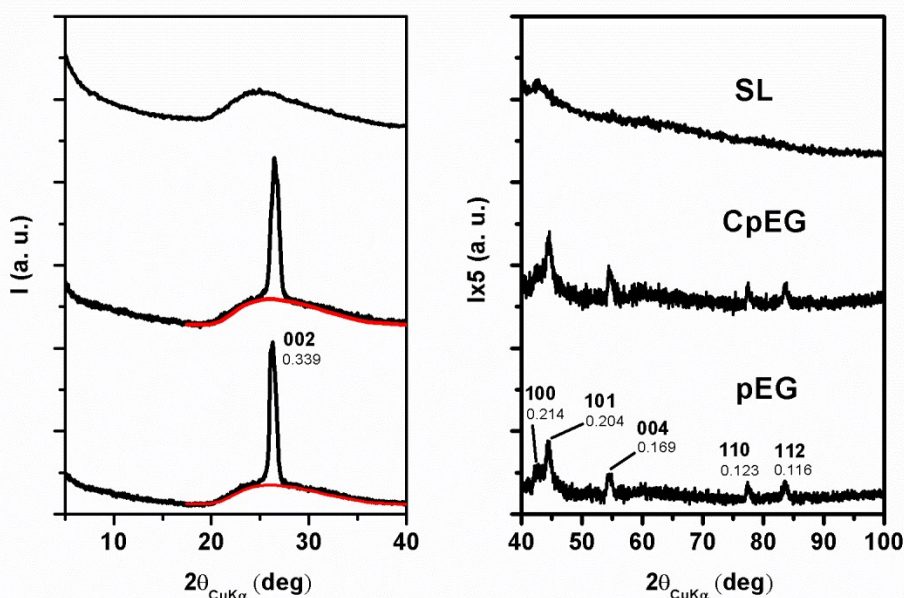
Figure 1S. X-ray diffraction patterns of pEG, CpEG and SL samples.

The WAXD patterns of the samples pEG and CpEG show the intense 002 reflection, corresponding to an interlayer distance of 0.339 nm; all the observed reflections for the samples pEG and CpEG are indicated in Table 1S, in which the observed XRD peak d-spacings are compared to the expected hexagonal graphite. Data shown in Table 1S indicate that the crystalline fraction of the exfoliated graphite is the most common form of graphite in nature. In fact, the values in the column of the "difference" indicate that it is hexagonal graphite with ABAB stacking of layers.

Table 1S. Observed XRD peak d-spacings of sample G and comparison to the expected hexagonal graphite.

Experimental d-spacings (Å)	(hkl)	Theory*	Difference
3.39	(002)	3.38	0.01
2.12	(100)	2.14	-0.02
2.08	(101)	2.04	0.04
1.70	(004)	1.69	0.01
1.23	(110)	1.23	0

*Theory values were found in ref. 14.

The surface area of the three sizes of exfoliated graphite particles were measured and are summarized in Table 2S, where the percentage of exfoliated phase is shown for all the analyzed samples. The percentage of

exfoliated phase was considered as the amorphous phase calculated using the equation (eq. 2) of the section 4.2 "*Characterization*" .

This assumption seems excessive if we consider only the structural analysis carried out by X-ray diffraction. Actually, this assumption has been made following a careful comparison between structural and morphological data. In fact, no amorphous carbonaceous materials different from graphene layers and/or graphitic blocks were observed by means of TEM, AFM and SEM investigation.

The crystallite coherence lengths perpendicular to reflection planes 002 (*D*002) were calculated in accord with the Scherrer's equation [1] for the two samples pEG and CpEG of partially exfoliated graphite, the obtained values are shown in Table 2S together with the values of Brunauer-Emmett-Teller specific surface area (S_{BET}).

Table 2S. Surface area, percentage of exfoliated phase, crystallite coherence lengths perpendicular to reflection planes 002 (*D*002) and crystalline phase of partially exfoliated graphite (pEG and CpEG samples) and completely exfoliated graphite (SL sample).

Sample	Surface Area (m^2/g)	Exfoliated Phase Xa (%)	D_{002} (nm)	Crystalline Phase Xc (%)
pEG	14.7	56	12.0	44
CpEG	16.3	60	9.8	40
SL	278	100	-	0

Data shown in Table 2S highlight that no relevant difference are detected in the structural parameters of samples pEG and CpEG, in particular sample CpEG shows a very small increase in the exfoliated phase (7%) and surface area (11%) with respect to sample pEG as described in the main text.

From Scherrer's equation, the average in the number of layers can be obtained using the following equation [2]

$$\text{Number of layers} = D_{002}/d_{002} \qquad \text{eq.1}$$

Considering the value of 3.39 Å for the d-spacing of the reflection (002), a number of about 35 and 29 layers was calculated for pEG and CpEG samples.

A visual observation of the analyzed samples is shown in Figure 2S.
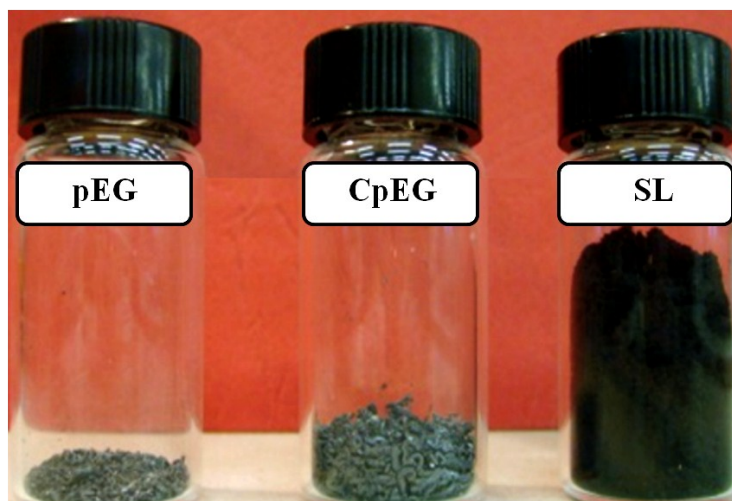
Figure 2S. Visual observation of the pEG, CpEG and SL samples.

The visual observation refers to the same amount of nanofiller (0.026 grams). It gives an idea of the difference in volume which is only slightly different for the samples pEG and CpEG, whereas a strong increase in the case of the sample composed of completely exfoliated graphite is observed.

Spectroscopic investigation

Raman Spectroscopy

SL powder sample was characterized by Raman spectroscopy. Figure 3S shows the Micro-Raman (MR) spectra recorded at the edge and on the basal plane of the SL sample.
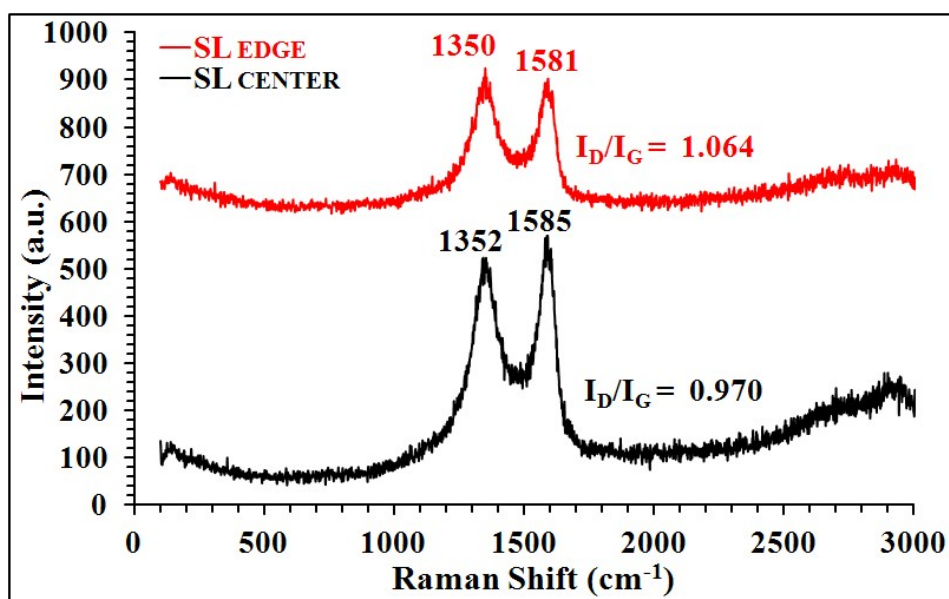

Figure 3S. Micro-Raman spectra recorded at the edge and on the basal plane of the SL sample.

In contrast with pEG and CpEG samples, SL spectrum shows a broad strong D band centered at 1350-1352 cm^{-1} with I_D/I_G ranging between 1.064 (at the edge) and 0.970 (within the basal plane of a the large layer).

As described in the main text the D-band at ~ 1350 cm^{-1} is identified with defects present in the carbon aromatic structure. The observed D peak also in the center of graphene layers in the spectra of SL sample proves the presence of a significant number of defects on the entire layer. In this interpretation of the spectra we do not ascribe the intense D band to the armchair structures; the reason for this will be further clarified considering the other characterizations performed on the nanofillers. The spectra of SL sample shows a relevant change in the shape and intensity of the 2D peak compared to the spectra of pEG and CpEG samples shown in Figure 1 of the main text. In particular, the 2D peak consists of two components $2D_1$ and $2D_2$ [3-4].

It was highlighted that a decrease in layers leads to a significant increase of the relative intensity of the lower frequency $2D_1$ peaks [5]. For more than 5 layers, the Raman spectrum becomes hardly distinguishable from that of bulk graphite as for samples pEG and CpEG. The profile of the G' peak and the relative intensity of $2D_1$ and $2D_2$ signals prove that the sample SL is prevalently composed of a number of layers equal or less than 3. This very low number of layers also explains the visual observation and the morphological feature of the SL sample and then the presence of the D band; in fact, the D band is observed to strongly increase with decreasing the number of layers. Graphene layers with a very low number of layers show to be less rigid and bend easily (in the next section "*Morphological Characterization*" of this *Supplementary Content*, we will see that this structural and morphological characteristic strongly affect the distribution of graphene layers inside the epoxy mixture and consequently the electrical performance). It is worth nothing that morphological investigation of the SL sample shows a very large number of layer narrow folding; the deformation from the planarity is expected to be associated with defect, or sp^3 hybridized carbon atoms that should cause an increase in the intensity of D-band (in our experience, this effect is relevant in the case of few (1-3) layers of graphene characterized by large surface area). On the other hand, these defects are always present in completely exfoliated graphite in the form of bulk sample. In fact, without defects and then functional groups chemically bonded to the graphene layers that act as local spacers, graphene layers (in the completely reduced form) tend to reassemble to form again graphitic materials.

The elementary analysis of SL sample, reported in Table 3S (together pEG and CpEG samples for comparison), indicates for SL the presence of large amount of oxygen, which is about 68 times higher than that of sample pEG and 3 times higher than that of sample CpEG. Data shown in table 3S also highlight that pEG appears to be the sample with the smallest number of functional groups, in fact the value of the ratio C/O is the highest one. The more functionalized sample is SL, whereas sample CpEG shows a ratio C/O which is 23 times smaller than that of EG sample.

Table 3S. Results of elemental analysis and BET measurements on anhydrous samples of pEG, CpEG and SL.

Sample	Elemental composition (%wt.)					
	C	H	N	O	S	C/O
pEG	99.5	0.1	0.0	0.4	0.0	248.7
CpEG	91.3	0.2	0.0	8.5	0.0	10.7
SL	66.8	1.2	4.9	27.1	0.0	2.5

Infrared Spectroscopy

Results of elemental analysis are confirmed by the FTIR spectra of Figure 4S, where pEG, CpEG and SL samples are shown.
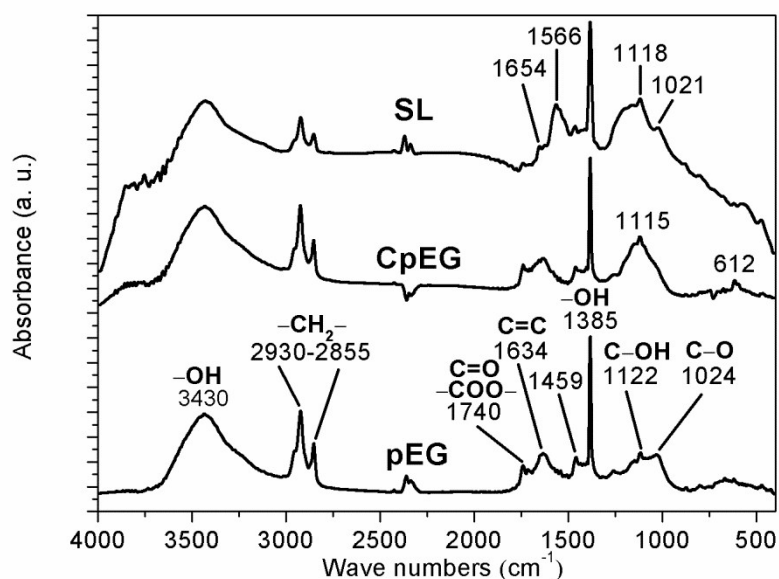
Figure 4S. FTIR spectra of the pEG, CpEG and SL samples.

As previous illustrated, all FTIR spectra show the presence of oxygenated functional groups (mainly carboxylic, hydroxyl and epoxide), whose concentration is slightly lower in the pEG sample (see main text). The presence of different type of oxygen functionalities was confirmed by the bands at 3430 cm^{-1} (O-H stretching vibrations), at 1730 - 1740 cm^{-1} (stretching vibrations from C=O), at 1627-16335 cm^{-1} (skeletal vibrations from unoxidized graphitic domains), at 1220 cm^{-1} (C-OH stretching vibrations – most of all in SL sample – as shoulder on the left of the band at 118 cm^{-1}), and at 1024 cm^{-1} (C-O stretching vibrations). The

profile of CpEG spectrum in the range 1000- 1250 cm^{-1} is more similar to SL sample than that of pEG sample. In particular, the spectra of pEG and CpEG samples differ from SL spectrum for the more intense signal at 1740 cm^{-1} due to the C=O stretching of the carboxyl groups. Another difference between pEG, CpEG samples and SL sample is the profile of the signals between 1000 and 1300 cm^{-1}; the shoulder on the left of the band at 1118 cm^{-1} indicates a major concentration of hydroxyl groups on SL sample. In addition in SL sample the signal at 1566 cm^{-1} is most likely due to the major concentration with respect to pEG and CpEG samples of aromatic substituted aromatic rings. pEG and CpEG samples show a quite similar profile of the bands except for profile of the peaks between 1000 and 1300 cm^{-1}. In fact in CpEG sample we can observe the more intense peak at 1115 cm^{-1}. As described in the main text, this peak is most likely due to the presence of O-C-C stretching of aromatic esters. In fact, it is worth noting that C-C-O, and O-C-C stretches for aromatic ester fall into different ranges than saturated esters [6].In particular, the conjugation modifies the wavenumbers of the ester signals and the O-C-C stretch of aromatic esters falls between 1130 and 1100 cm^{-1}. This result will reasonably lead to expect that in phase of preparation of CpEG, some of the –OH groups of carboxyl acids condense with -OH hydroxyl groups to form aromatic ester groups according with the figure of scheme 1Sa. It is worth noting that carboxyl groups are expected to be mainly located at the edge of graphene layers or graphitic blocks [7-9]; then the previous results together with the elemental analysis highlight that sample CpEG is characterized by the higher concentation of carboxilated groups at the edge of graphene layers or graphitic blocks, which can create self-assembly structures through intermolecular hydrogen bonding that in some regions can also form aromatic ester groups bonding different graphene layers/blocks as illustrated in scheme 5d of the main text.

Thermogravimetric Analysis (TGA)

Figure 5S shows the TGA thermograms for pEG,HEG and SL samples (at heating rate of 10°C min^{-1}) under air atmosphere.
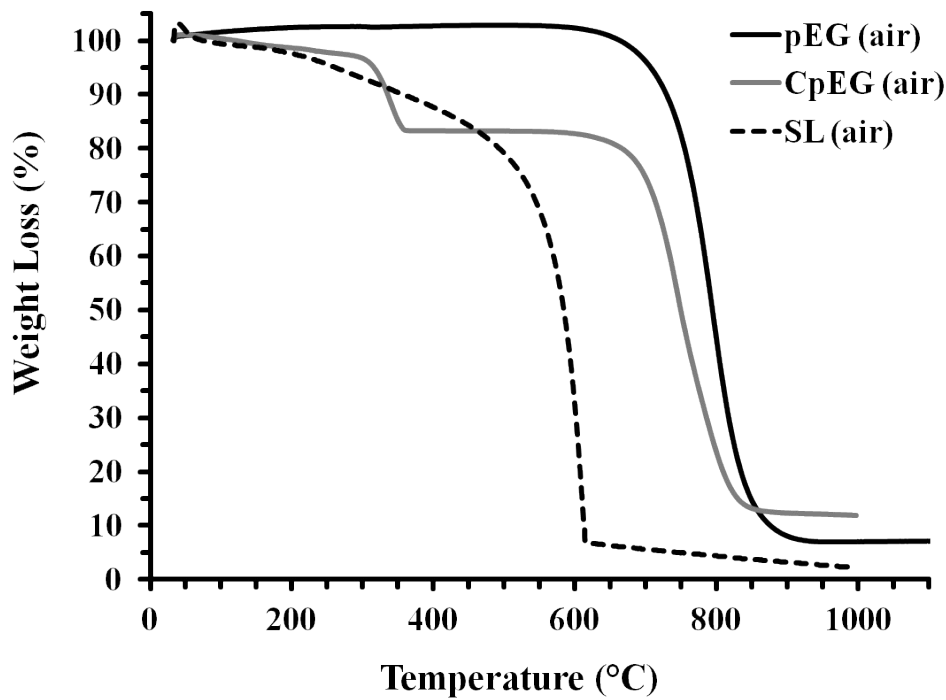
Figure 5S. TGA thermograms for pEG, CpEG and SL samples.

SL sample starts to lose weight first gradually around 90-100°C highlighting a gradual loss of water due to the large number of hydroxyl groups present on the basal planes and edges of graphene layers.

Exfoliated graphite: morphological investigation

SEM investigation of the exfoliated graphite pEG, CpEG and SL sample was performed to analyze the morphology of each nanofiller before its incorporation into the epoxy mixture. Figure 6S shows SEM images of pEG, CpEG and SL samples respectively. SEM images of pEG and CpEG samples have been partially discussed in the main text. A very important aspect related to the morphology of these samples is that no amorphous domains are observed in both samples, this assures that X-ray evaluation is accurate. Sample SL shows a very wrinkled morphology where the flat flake-like morphology is completely lost. The wrinkled morphology is clearly seen in the TEM image of Fig 6Sb where we can see single layers of large surface area highly wrinkled and folded.
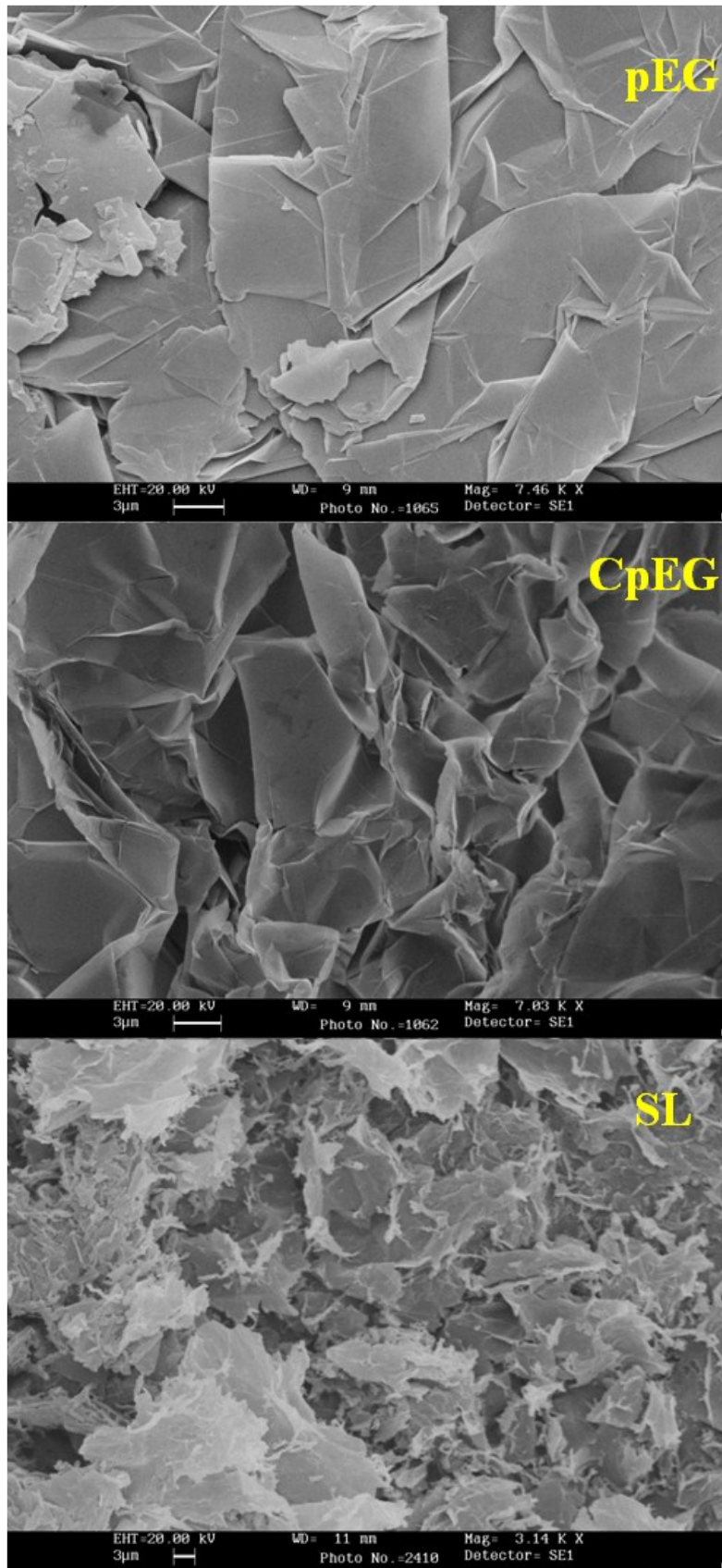
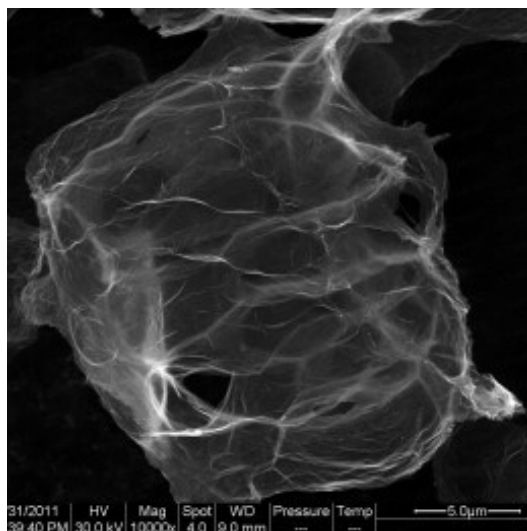**Figure 6S.** SEM images of pEG, CpEG and SL samples.

Figure 6Sb. TEM images of SL sample.

Nanofilled Resin characterization

Morphological Characterization

The morphology of samples filled with pEG and CpEG samples has been already discussed in the main text. The morphology of the sample nanofilled with SL particles (0.5 wt%) is shown in Figure 7S. The sample nanofilled with SL nanoparticles were etched with the same etching procedure of the sample pEG and CpEG; nonetheless only in the high-magnification images it is possible to clearly observe the nanofiller features inside the resin. In fact, in this case, graphene layers show a strong tendency to screw up and then distributed locally only in some regions. This effect can be clearly seen in the images on the bottom of Figure 7S, whereas the image on the top gives information on a more global distribution of the nanoparticles. It is worth noting that SL nanoparticle contains many hydroxyl groups on the basal planes which can condense during the preparation of the sample (mixing temperature, sonication etc..) leading to covalent bonds and strong attractive interactions that promote the crumpling around it-self. This last mechanism, together with the very low concentration of carbon atoms with sp^2 hybridization does not favors the electrical conductive paths, in fact the electrical conductivity of the resin filled with SL graphene is approximatively equal to the unfilled sample.

Figure 7S. SEM images at different magnification of the fracture surface of nanofilled resin at loading rate of 0.5 % by weight of SL sample.

Structural Characterization

Figure 8S shows XRD patterns of: TBD unfilled epoxy resin, TBD-pEG 1%wt, TBD-pEG 2%wt TBD-pEG 4%wt, TBD-pEG 6.5%wt nanofilled epoxy composites at different percentage by weight of exfoliated graphite (pEG).
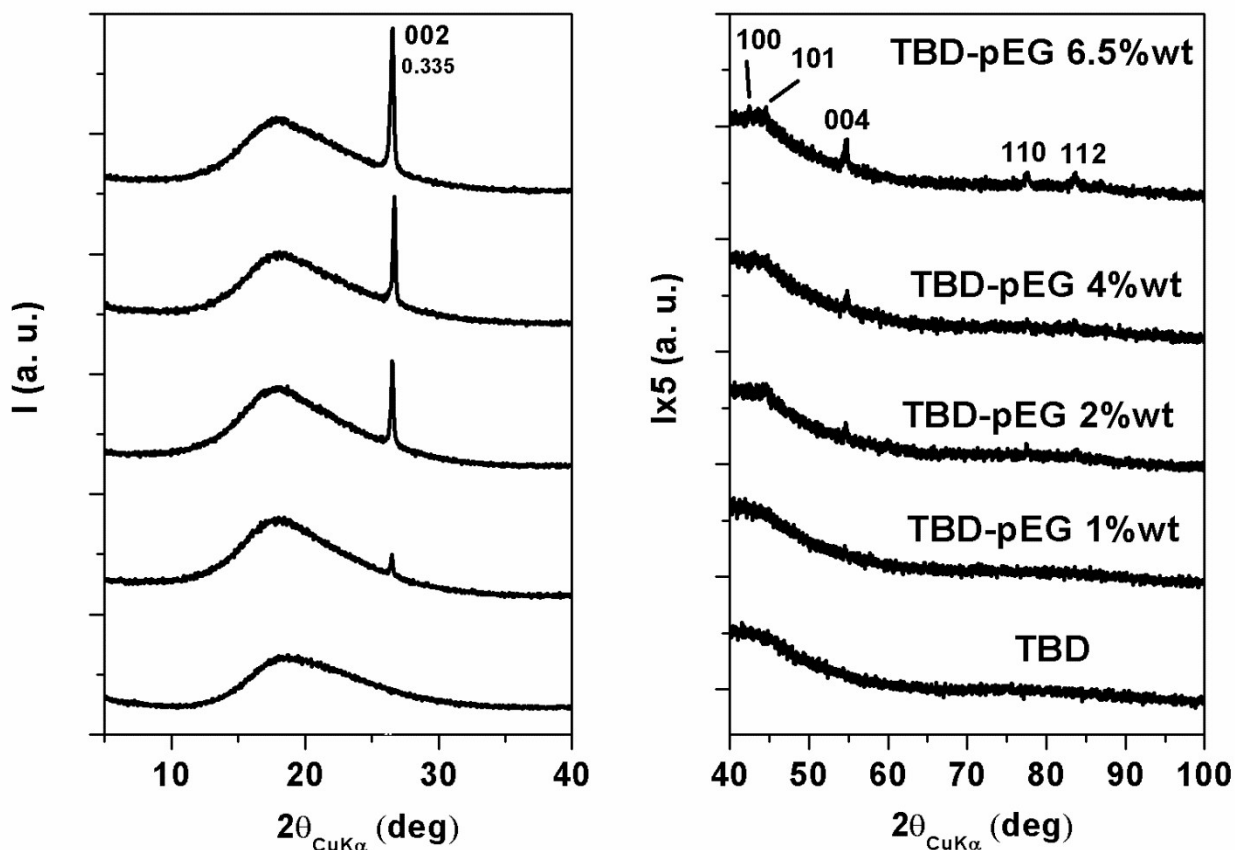

Figure 8S. XRD patterns of: TBD unfilled epoxy resin, TBD-pEG 1%wt, TBD-pEG 2%wt, TBD-pEG 4%wt, TBD-pEG 6.5%wt nanofilled epoxy composites at different percentage by weight of exfoliated graphite (pEG).

As discussed in the section a number of about 36 layers was calculated for the pEG sample.

In all the nanofilled samples, composites with TBD, the crystal size of pEG in the direction perpendicular to the planes 002 is 40-45 nm, therefore, during the process of formation of the composite, the pEG particles re-aggregate and the crystals become more ordered with respect to the nanofiller alone. Furthermore, the reflection 002 shows a shift from 26.3 in the pristine pEG to 26.6 degrees of 2 theta in the composites. Figure 9S shows the XRD patterns of the epoxy mixture TBD, TBD-pEG 2%wt, TBD-CpEG 1.8%wt, TBD-SL 0.5%wt.
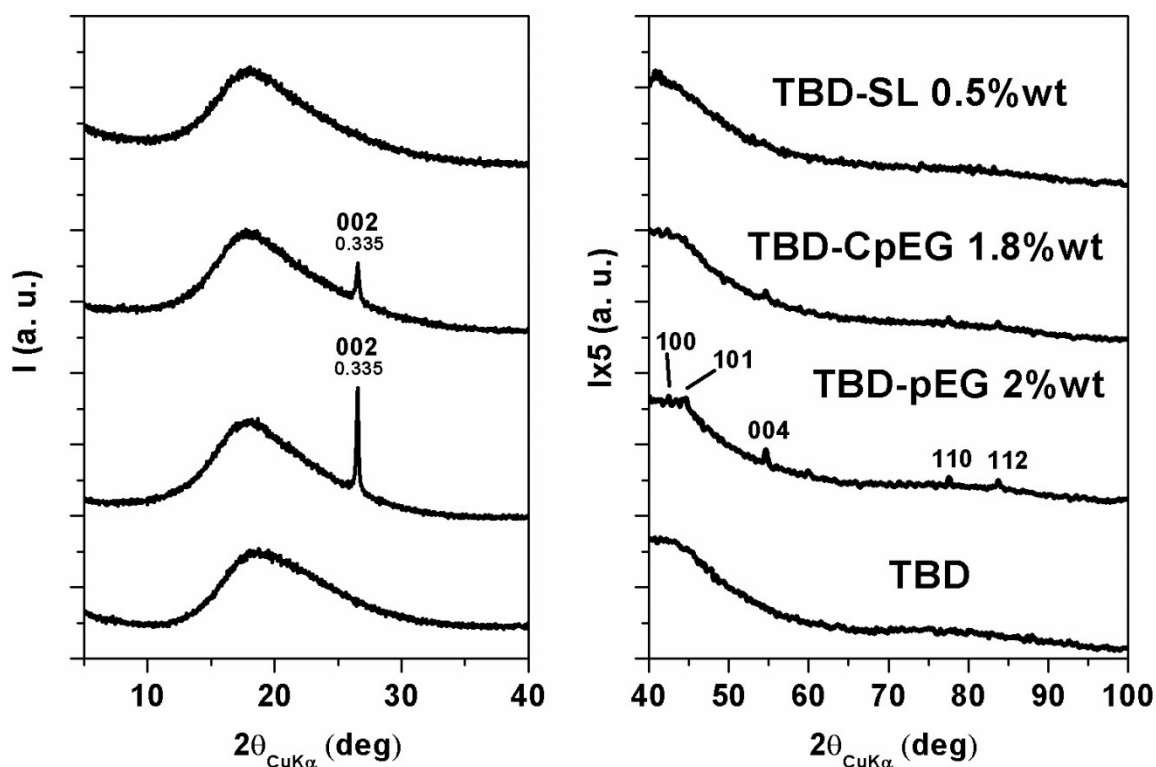
Figure 9S. XRD patterns of TBD, TBD-pEG 2%wt, TBD-CpEG 1.8%wt, TBD-SL 0.5%wt.

Data shown in Figure 9S highlight that no cristallization effects are detected for the SL sample due to the complete exfoliation and the absence of re-assembling phenomena prevented by the high value in the degree of functionalization.

Thermogravimetric characterization

Figure 10S shows the thermogravimetric curves in air of the epoxy formulation nanofilled with pEG and CpEG. A two-step thermal degradation process can be observed for all the samples. The first stage of thermal degradation of the nanofilled samples substantially occurs in the temperature range of 380–480°C, highlighting a stabilizing effect of the graphene-based nanoparticles in the first stage of the degradation; in fact the unfilled sample TBD shows a slight weight loss (~5%–6%) in the temperature range between 150 and 380°C. The end of the first stage at about 460°C involves the same mass loss for all the nanofiller. The beginning of the first stage is most probably due to degradation processes which do not involve oxygen (dehydration, random scission etc), whereas the second step is strongly dependent on the oxygen availability. This hypothesis is supported by the different trend of the thermogravimetric curves in inert (N_2) atmosphere (Figure 11S). There are two distinct and well-separated turns also for TGA curves in nitrogen; the first step is in the same temperature range, whereas the second step is much slower with respect to the degradation in air.

A very interesting result is the different mass loss at the end of the first stage; it is between 60–70% in nitrogen and 45–50% in air, this effect is not influenced by the presence of nanofiller.
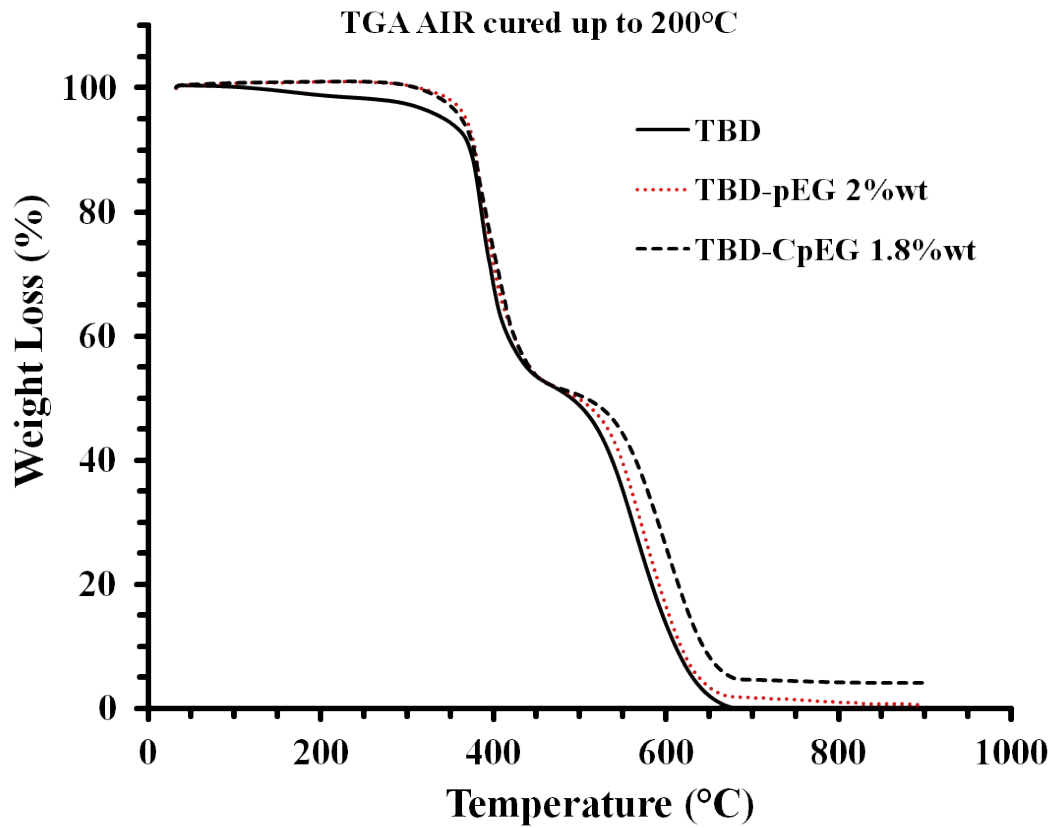

Figure 10S. Thermogravimetric curves in air of the pure epoxy formulation and the formulation nanofilled with pEG and CpEG.
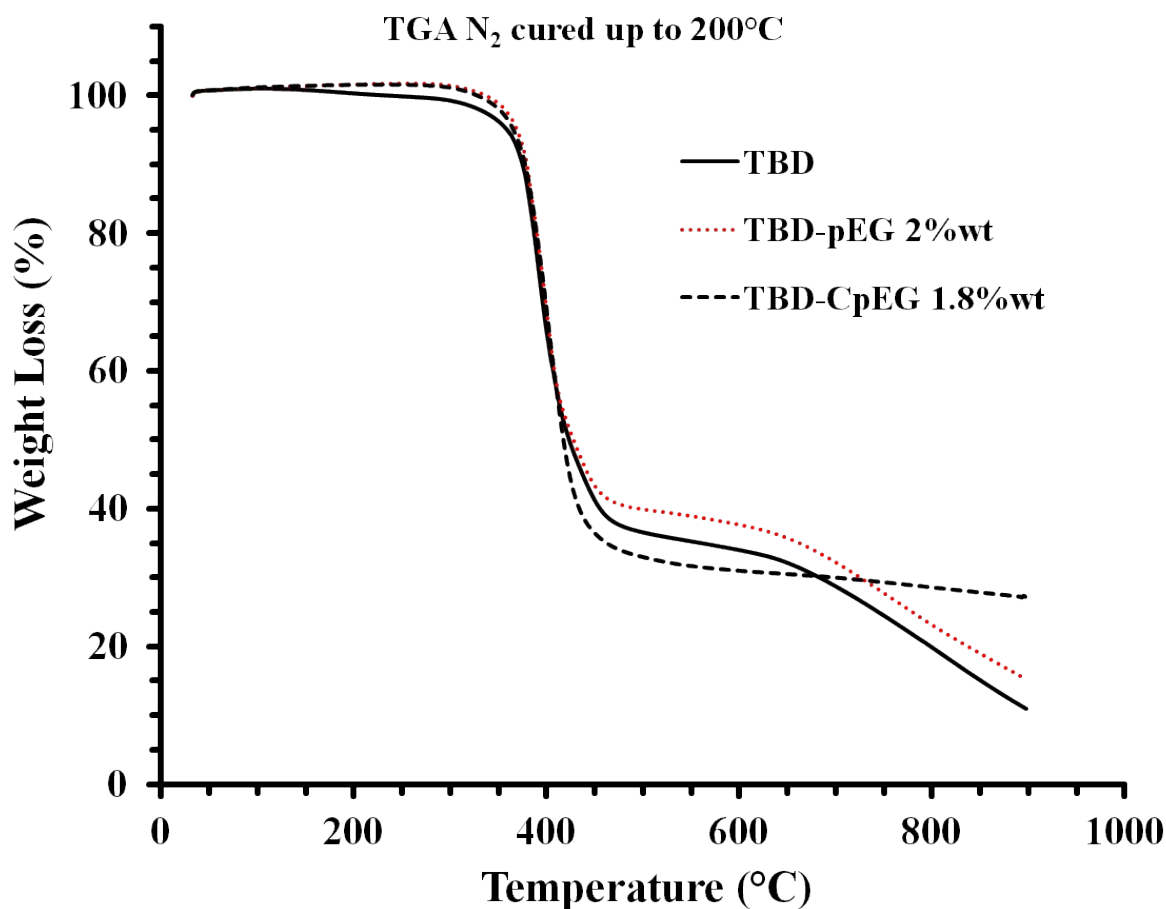
Figure 11S. Thermogravimetric curves in nitrogen of the pure epoxy formulation and the formulation nanofilled with pEG and CpEG.

Considerations

The current status of epoxy/graphene nanocomposites was analyzed with the aim to find effective strategies to transfer some of excellent physical properties of graphene layers to epoxy matrices. The evaluation of edge structures of very similar graphene-based materials, differing only for the concentration of carboxylated group on the edges, highlights that the effect on the electrical and mechanical properties is impressive. The chemistry of graphene edges strongly affects the physical properties of the resin where these nanoparticles are embedded. Integrate characterizations techniques (RX, Micro-Raman, FTIR, TGA, SEM) can facilitate our understanding of graphene-based materials and their development towards applications.

In particular, with samples constituted by roughly 50% of graphite with a correlation length perpendicular to the structural layers ranging between 12 nm e 9.8 nm and 50% of exfoliated graphene, for standard epoxy composites, electrical percolation threshold can be achieved with nanofiller concentration less than 0.5% by weight. This value of nanofiller concentration allows to reach dc electrical conductivity raging between 1-2

S/m. The good electrical and mechanical performance was ascribed to self-assembly mechanisms determined by attractive interactions between edge-carboxylated graphene particles. This hypothesis is reflected in the different electrical behavior of Epoxy based composites including two partially exfoliated graphite samples, differing essentially only for the content of carboxylated groups. These two samples have shown an electrical percolation threshold which decrease from 3wt% down to 0.3 wt%, as the carboxylated group content increases up to 10 wt%. A self-assembly of layers due to the attractive interactions between edge-carboxylated graphene particles was found to favor the electrical percolative paths. Edge-carboxylation also increases the nanofiller/epoxy matrix interaction determining a relevant reinforcement in the elastic modulus. This controllable feature of the nanoparticles can be an alternative parameter to design epoxy resins where high electrical conductivity is required at very low filler concentration. A sound choice of the nanofiller nature allows to drive the changes in the nanocomposite properties towards the set goals. A very important result of this study is that the values detected for the electrical parameters were found very similar to those obtained with mono-dimensional shaped nanofillers in the same epoxy matrix (Fig. 15S) where the electrical properties found for the nanocomposites loaded with CpEG samples, are compared to those achieved for composites based on the same epoxy matrix and employing other typical conductive fillers, i.e. multi-walled nanotubes, (MWCNT), pristine (CNF1100) and heat-treated (CNF2500) carbon nanofibers as shown in the histogram of Figure 12S.
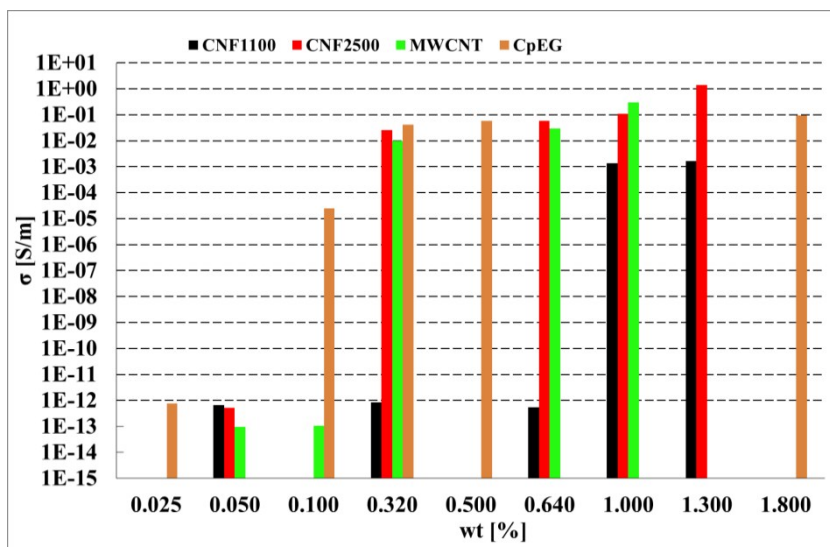

Figure 12S. Comparison of electrical conductivity as function of the filler concentration for different type of carbon based particles.

The electrical percolation threshold for the CpEG samples is the lowest among all the different nanofillers adopted with this type of epoxy resin. In general, the electrical conductivity is very similar for heat-treated CNFs and MWCNTs. In particular, for the weight percentage of 0.32 wt%, the epoxy resin filled with CpEG presents a slightly higher electrical conductivity than that obtained with the other fillers.

Furthermore, a filler concentration of only 0.5% wt of CpEG is sufficient to reach values of electrical conductivity comparable with those obtained by using nanotubes or heat-treated fibers with a higher content, i.e. 0.64% wt. In the explored range of filler loading, the higher value for the conductivity is achieved for the epoxy mixture filled by CNF2500 (at 1.30 %wt).

Acknowledgments

References

1. H. Tadokoro, Structure of Crystalline Polymers, John Wiley& Sons, New York (1979).
2. H. M. Ju, S. H. Huh, S. H. Choi and H. L. Lee, Structures of thermally and chemically reduced graphene, *Materials Letters*, 2010, **64**, 357-360.
3. C. Thomsen and S. Reich, Double Resonant Raman Scattering in Graphite, *Phys. Rev. Lett.*, 2000, **85**, 5214-5217.
4. P. Venezuela, M. Lazzeri and F. Mauri, Theory of double-resonant Raman spectra in graphene: Intensity and line shape of defect-induced and two-phonon bands, *Phys. Rev. B*, 2011, **84**, 035433 (25 pp).
5. A. C. Ferrari, J. C. Meyer, V. Scardaci, C. Casiraghi, M. Lazzeri, F Mauri, S. Piscanec, D. Jiang, K. S. Novoselov, S. Roth and A. K. Geim, Raman Spectrum of Graphene and Graphene Layers, *Phys. Rev.Lett.*, 2006, **97**, 187401-4.
6. Brian C. Smith, Infrared Spectral Interpretation: A Systematic Approach, December 10, 1998 by CRC Press, 288 Pages, ISBN 9780849324635, printed in United States of America.
7. S. Gadipelli and Z. X. Guo, Graphene-based materials: Synthesis and gas sorption, storage and separation, *Progress in Materials Science*, 2015, **69**, 1-60.
8. G. Eda and M. Chhowalla, Chemically Derived Graphene Oxide: Towards Large-Area Thin-Film Electronics and Optoelectronics, *Advanced Materials*, 2010, **22**, 2392-2415.
9. D. R. Dreyer, S. Park, C. W. Bielawski and R. S. Ruoff, The chemistry of graphene oxide, *Chem. Soc. Rev.*, 2010, **39**, 228-240.